applied sciences

MDPI

Article

Relationship between Fault Level and System Strength in Future Renewable-Rich Power Grids

Rafat Aljarrah [1], Mazaher Karimi [2,*], Hesamoddin Marzooghi [3], Sahban Alnaser [4], Murad Al-Omary [5], Qusay Salem [1] and Salman Harasis [6]

1 Electrical Engineering Department, Princess Sumaya University for Technology, Amman 11942, Jordan
2 School of Technology and Innovations, University of Vaasa, FI-65200 Vaasa, Finland
3 Team Leader Power Systems Studies, Power Systems Consultants Australia Pty Ltd. (PSC), 3 Spring Street, Sydney, NSW 2000, Australia
4 Department of Electrical Engineering, The University of Jordan, Amman 11942, Jordan
5 Energy Engineering Department, German Jordanian University, Amman 11180, Jordan
6 Electrical Power and Mechatronics Engineering Department, Tafila Technical University, Tafila 66110, Jordan
* Correspondence: mazaher.karimi@uwasa.fi

Abstract: The fault level is used as a simple indicator for scanning the system strength in power systems. To an extent, this has proven its efficacy in classical power systems based on synchronous generation (SG). However, power electronics-based renewable energy sources (RESs), due to their controlled and limited fault current contribution, may affect the impedance, fault level, and system strength in a non-linear manner. Hence, this raises a question about the validity of using the fault level as a measure reflecting the system strength in future grids. This paper intends to shed light on the above question by examining the correlation between the fault level and the system strength in future grid scenarios. This is achieved in two steps: first, by employing the measure-based Thevenin impedance for fault level estimation in renewable-rich grids, and second, by comparing these estimated fault levels with those obtained from steady-state and dynamic simulations. While the results have demonstrated the suitability of using the fault level for system strength scanning in scenarios of low penetration of RESs, they revealed that such a tool might be misleading with very high RES penetrations. The findings have been verified using the adjusted IEEE nine-bus test system in DIgSILENT PowerFactory.

Keywords: fault level; system strength; Thevenin impedance; renewable energy sources

Citation: Aljarrah, R.; Karimi, M.; Marzooghi, H.; Alnaser, S.; Al-Omary, M.; Salem, Q.; Harasis, S. Relationship between Fault Level and System Strength in Future Renewable-Rich Power Grids. *Appl. Sci.* **2023**, *13*, 142. https://doi.org/10.3390/app13010142

Academic Editor: Roberto Zivieri

Received: 21 November 2022
Revised: 13 December 2022
Accepted: 19 December 2022
Published: 22 December 2022

1. Introduction

Power systems are moving towards integrating higher penetration of renewable energy sources (RESs). Simultaneously, this is accompanied by the decommissioning of large central synchronous generators (SGs). As most RESs are connected to the grid through power electronic (PE) devices, they have different characteristics and limitations in terms of inertia and fault level contribution to the grid [1,2]. This in turn would negatively affect the system from the strength point of view. In other words, the increased penetration of PE-based RESs may result in weaker future grids. Note that the term 'system strength' in this research refers to the system impedance that characterizes the capacity of a system to maintain the voltage in response to changes in the current (e.g., switching events or load changes). Thus, lower impedance, i.e., a higher fault level, implies that the power system is stronger at that point and vice versa. This issue has started to capture the attention of researchers and system operators (transmission system operators (TSOs) and distribution network operators (DNOs)) due to its severe impact on the operation and control of the grids [3–5]. Therefore, continuous monitoring of the system strength, especially in future system scenarios with high penetration of PE-based RESs, is required. In this regard, the fault level, being directly related to the system impedance at the faulty point, has been

adopted as a helpful tool to measure the system strength (i.e., the system impedance) locally around the power grid [6,7]. For instance, a higher fault level point indicates a lower system impedance and a closer point to the generation centre.

Although system impedance, also referred to as Thevenin impedance, when measured at steady-state conditions at a certain node may differ from that concerning dynamic fault conditions, these two values might be almost the same in classical power systems, specifically at load buses [8]. This is supported by the assumption that the sub-transient and transient effects of synchronous machines can be neglected. Therefore, estimating the system impedance, to an extent, is employed to calculate the fault level and vice versa. Thus, the efficacy of the fault level scanning tool has been proven in classical power systems dominated by SGs, as the fault level, to an extent, would represent the system impedance. With the increased penetration of PE-based RESs, such tools may be invalidated in future grids. This might be attributed to the controlled fault current response from those non-synchronized RESs opposing the situation of classical SGs that are directly coupled with the grid. RESs not only have limited fault contribution, but they also have different fault signatures and characteristics, mainly due to the their converter's controllers and protection setup during the faults [9]. Moreover, these RESs cannot be modelled as voltage behind an impedance, which is the case with SGs. Hence, the increased penetration of RESs when accompanied by decommissioning of large SGs may lead to the grids being operated under lower fault level conditions. Regardless of the low fault level contribution, depending on the technology, the controllers, and the fault-ride through requirements set by grid codes, RESs may still contribute partially to the system strength in normal operation conditions. However, this might not be captured by using the fault level scanning tool. This necessitates the need to better understand the correlation between the fault level and the system strength represented by the system impedance.

Traditionally, using the Thevenin impedance has been employed for steady-state fault calculations by most standards, such as IEEE and IEC standards [10,11]. This is not only due to its simplicity, but also due to the accuracy achieved in estimating the fault currents. This is because of the direct and linear (inversely) relationship between the impedance and the fault current flowing at the point of study. Such relationship is attributed to the physical behaviour of the classical SGs during faulty conditions. These SGs provide a time-decaying fault current which is inversely related to their impedance seen during the fault. SGs' fault currents are usually of very high values which go multiple times above its rating (e.g., up to six p.u.). Nevertheless, the Thevenin equivalent method may not provide the same accuracy when the fault current comes to the systems from RESs with different characteristics and limited fault current contributions when compared with SGs (e.g., up to 1.4 p.u.) [9]. Hence, these Thevenin-based methods attempted to modify their approach to better include the impact of such RESs in fault calculation methods. For instance, IEC 60909 standards suggested that the PE-based RESs should be modelled as a current source with infinite impedance.

Aside from fault calculation standards, many studies have attempted to map the system strength and the fault level in power systems. These studies can be categorized into two main classes:

(1) Those that studied the application of measurement-based methods for Thevenin impedance and fault level estimation [12–16]. Although such studies provided a valuable insight, they were mostly analysing the system impedance and the fault level in classical/existing power systems without considering the impact of very high RES penetration.

(2) Those focused on employing of the fault level and the short circuit ratio (SCR) for evaluating the system strength for PE-based RES integration purposes [17–22]. Such studies assess the strength of the AC/DC connection when integrating RESs. Some of these studies have suggested modified SCR-based metrics for better scanning of the system strength. However, they were restricted to the point of common coupling (PCC) and did not consider the fault current contribution from RESs. Moreover, they

have not clearly pointed to the impact of the fault contribution from PE-based RESs on those suggested metrics.

In recent literature, researchers have started to raise questions on the accuracy of employing the fault level for reflecting the traditional concept of Thevenin impedance and the system strength in future renewable-rich scenarios [23,24]. For instance, researchers in [23] have concluded that the classical definitions of grid strength based on short-circuit power and Thevenin impedance are inadequate as they may fail to describe the system behaviour. The work in [24] argues that a fault level may not be a valid measure of the equivalent system impedance, i.e., the system strength in systems with large-scale integration of PE-based RESs.

In this paper, we aim to examine the effectiveness of using a fault level-based approach as a system strength scanning tool that reflects the Thevenin impedance in future grid scenarios with high penetration of RESs. (i.e., PE-based generators). Our analysis focuses on achieving a better understanding of the correlation between the fault level and the system strength in such scenarios. The work in this paper is divided into two steps: first, estimation of the fault level in renewable-rich grids by utilizing the measure-based Thevenin impedance, and second, comparison between these estimated fault levels with those obtained from stead-state and dynamic simulations. Then, depending on the matching degree of those two categories of results, the fault level will be reassessed as a system strength scanning tool in future power grids with high penetration of RESs.

The rest of the paper is structured as follows: Section 2 introduces the difference between the typical characteristics of fault currents from SGs and PE-based RESs. Section 3 presents the concept of a measurement-based estimation of the power system impedance based on load change and capacitor switching methods. Section 4 revises the up-to-date fault calculation in renewable-rich grids according to IEC 60909 standards. Section 5 discusses the simulation results and validates the accuracy of the utilized methods against the dynamic simulations, and finally, Section 6 concludes the paper.

2. Typical Characteristics of Fault Current of SGs versus PE-Based RESs

The SGs are considered as the main source feeding the fault level in conventional power systems. Due to their physical behavior, the fault currents fed from SGs are time-decaying currents with a very high initial contribution (i.e., sub-transient current). The initial fault contribution is followed by a lower level of transient contribution before reaching the lowest level of fault current components represented by the steady-state component. Figure 1 shows the typical fault current signature of SG and RESs (i.e., type-four wind). In order to mimic the behavior, SG is usually modelled as a voltage behind and impedance for fault calculations. The impedance, which is mainly characterized by the reactance of the generator, has three different values that vary to represent the above-mentioned components.

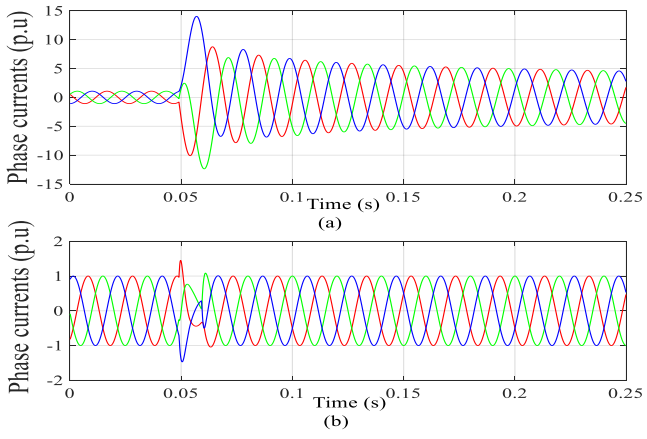

Figure 1. Typical fault current signature of a 50 MVA generation unit. (**a**) SG (**b**) type-four wind [2].

This behavior is due to the PE interface utilized in their converters. Generally, RESs may have a fast transient that is followed by a limited steady-state fault component in response to the faults and voltage dip conditions [2]. Note that these RESs are usually accompanied by protection schemes that prevent high fault currents from passing through the converter to avoid stressing of the PE switches. In fact, it is not only the protection that affects the fault current contribution of RESs, but also the control strategy, the severity of the fault, and the fault-ride-through (FRT) requirements according to the grid code that is set by the grid operator.

3. Fault Level Estimation Using Measurement-Based Thevenin Impedance

The fault level is a quantity defined to represent the MVA associated with a three-phase symmetrical bolted short circuit current flowing at a faulty node. Once the short circuit current is known, then the fault level can be calculated according to Equation (1):

$$Fault\ Level\ (MVA)\ =\ \sqrt{3}\ V_N\ I_F \tag{1}$$

where V_N is the pre-fault line-line voltage of the point N in (kV) and I_F is the value of the three-phase symmetrical bolted short circuit current in (kA).

Note that this calculation process requires conducting a short circuit analysis to determine the value of the short circuit current at the node of interest. Alternatively, the fault level can be also captured by employing the Thevenin equivalent of the network seen from the node of interest as shown in Figure 2. Hence, the fault level can be expressed in Equation (2):

$$Fault\ Level\ (MVA)\ =\ \frac{V_N^2}{|Z_{th}|} \tag{2}$$

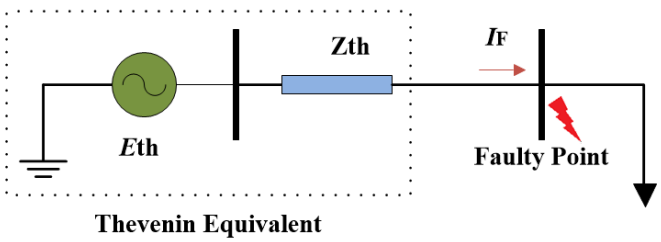

Figure 2. Thevenin equivalent of the system.

As mentioned earlier, some methods in the literature employ measurements for online estimation of the Thevenin impedance. This is undertaken mainly by measuring the voltage and current variations in response to active and reactive power (P and Q) variations due to a perturbation [8]. Depending on the source of the perturbation, the Thevenin impedance estimation methods can be categorized into two main groups: *passive* and *active*. The latter method can be also divided into two sub-categories: transient and steady-state, depending on the type of the event that caused the perturbation. Regardless of those categories, Thevenin impedance requires at least two consecutive measurements to be captured [25,26].

In this paper, to capture the Thevenin impedance that represents the system in steady-state conditions, two methods have been adopted to create the voltage/current variations for estimating the steady-state impedance of the system [8,27,28]. The estimated Thevenin impedance is then employed for fault level calculations These include: (1) Thevenin impedance measurement using step load change, and (2) Thevenin impedance measurement using switching events (e.g., capacitor bank switching). Note that these two measurement-based methods are supposed to be providing similar results when applied to the load buses. However, the capacitor bank switching method can be applied to any bus in the system, more specifically unloaded buses. While these might be converging into the same results in the conventional systems based on SGs only, they might lead to

different results with the presence of a high share of RESs. Hence, the assessment of these two methods is one of the expected findings of this paper.

3.1. Thevenin Impedance Measurement Using Step Load Change

Load side variations can be utilized to estimate the Thevenin impedance at the load nodes [29–31]. Note Figure 2 which shows the equivalent system at the load bus where the system side equivalent is kept unchanged. Any step change in the load side would be followed by a change in the voltage. By recording consecutive measurements of both the currents and the voltage before and after the load variations, the equivalent impedance at the load bus can be calculated as expressed in Equation (3):

$$\overline{E_{th}} = \overline{V_{L,i}} + \overline{Z_{th}} \times \overline{I_{L,i}} \tag{3}$$

Note that the variables in the above equation (voltages and currents) represent the actual RMS values measured in the positive sequence. While both $\overline{E_{th}}$ and $\overline{Z_{th}}$ are kept constant, any change in the current $\overline{I_{L,i}}$ would be accompanied by a change in the voltage $\overline{V_{L,i}}$. Hence, two consecutive measurements of two loading conditions (i.e., i = 1, 2) would lead to two different equations, as follows:

$$\begin{aligned} \overline{E_{th}} &= \overline{V_{L,1}} + \overline{Z_{th}} \times \overline{I_{L,1}} \\ \overline{E_{th}} &= \overline{V_{L,2}} + \overline{Z_{th}} \times \overline{I_{L,2}} \end{aligned} \tag{4}$$

By solving these two equations, the value of the Thevenin impedance can be calculated as follows:

$$Z_{th} = \left| \frac{\overline{V_{L,1}} - \overline{V_{L,2}}}{\overline{I_{L,1}} - \overline{I_{L,2}}} \right| \tag{5}$$

It is worth noting that the outcome of this method might be limited to cases where the system side is assumed unchanged during the measurements. In this regard, some literature can be found to account for source side variations [8], which is beyond the scope of this paper. However, it would be satisfied for the purpose of a steady-state Thevenin impedance estimation where variations are considered insignificant. In this work, a large step change in the voltage at the load bus is guaranteed for the purpose of improving the accuracy of this method. This voltage change is obtained by a large step change in the load that might be enough to neglect the continuous steady-state small variations in the source side. More specifically, the changes (5%, 10%, and 15%) are used and averaged to improve the accuracy of this method. This will be further discussed in the results section.

3.2. Thevenin Impedance Measurement Using Capacitor Bank Switching

Capacitor banks are usually utilized for steady-state voltage support at both transmission and distribution levels (often close to the large load center). By switching them on, capacitor banks can change the voltage level by injecting a reactive current at the bus where they are connected. Although this switching might be accompanied immediately by a transient inrush current, the steady-state voltage would be enhanced remarkably [32]. Both the transient current and resulting steady-state voltage step change are influenced by the system's strength, which is indicated by the Thevenin impedance (i.e., the fault level) at the connection point. For the purpose of this paper, which accounts only for steady-state conditions, the transient inrush current is not considered and the whole transient state is ignored. Note that less voltage changes result from capacitor banks switching at stronger buses (i.e., low equivalent impedance). Hence, similar to the load change method described earlier, capacitor banks switching events can be employed to estimate the Thevenin impedance at the node of connection. As depicted in Figure 3, the node at which the capacitor bank is connected can be represented by its Thevenin equivalent. Hence, by acquiring two sets of

measurements of the voltage and current before and after the capacitor switching event, we can simply calculate the Thevenin impedance as expressed in Equation (4):

$$Z_{th} = \left| \frac{\overline{V_{L,1}} - \overline{V_{L,2}}}{\overline{I_{L,1}} - \overline{I_{L,2}}} \right| = \left| \frac{\Delta V_L}{I_C} \right| \quad (6)$$

where I_C is the rated value of the capacitor current.

Note that the perturbation caused by the injected reactive current I_C should not result in a voltage beyond the steady-state voltage limits defined by the grid operator (e.g., ±5% of the nominal voltage). It is worth highlighting the applicability of this method for the estimation of the Thevenin impedance, not only at load buses but also at other unloaded buses at both transmission and distribution levels. By doing so, the obtained Thevenin impedance at the node of interest can then be employed to calculate the fault level MVA at the node of interest as previously expressed in Equation (2).

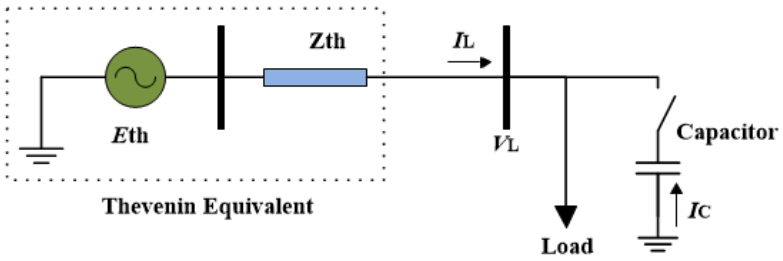

Figure 3. Thevenin equivalent of the system seen at the capacitor bank.

4. Fault Level Contribution of PE-Based RESs According to IEC 60909 Standards

The SC current contributions of PE-based RESs are limited and of different characteristics compared with those that can be observed from SGs. Due to the fast control response of the PE interfaces utilized in such RESs, they are modeled as current sources with fixed contribution according to the latest version of the IEC 60909 standards [10]. At first, the traditional Thevenin equivalent method is used in the fault calculation to determine the SC current without taking RESs into account. Then, the SC current contribution of the RESs is added to those calculated values using superposition. In other words, the SC contribution of PE-based RESs is not accounted for with the impedance model utilized for the SC current calculations. To account for their SC currents, PE-based RESs are modelled as current sources in the positive sequence with infinite impedances. It should be noted that the positive-sequence infinite impedance Z_{RES} is presumed to be shuntly connected; as a result, it is ignored and has no impact on the RESs fault contribution to the faulty bus. The value of the current source is typically inductive and it is usually provided by the manufacturer. Note that this value depends on several parameters, such as the converter overrating capability during the fault, the control strategy, and the FRT requirement. It is common to presume that the highest current injected by the PE-based RES, $IRES_{max}$, is limited to approximately 1–1.4 p.u. of the converter's rated current [9]. However, the SC contribution of the RESs at the faulty bus depends on both the transfer impedance between the RES source and the faulty bus, and the Thevenin equivalent impedance at the faulty bus, as expressed in Equation (7):

$$IRES_{SC} = \frac{1}{Z_k} \sum_{j=1}^{j=M} Z_{ij} \times IRES_{max} \quad (7)$$

where,

- M is the number of connected PV systems.
- $IRES_{max}$ is the maximum current source of the RES system connected to the jth bus.
- $IRES_{SC}$ is the total SC current contribution of all connected RESs.

- Z_{ij} is the transfer impedance between the bus j and the faulty bus i.
- Z_k is the equivalent impedance at the faulty bus k.

5. Results and Discussion

This section analyses the aforementioned methods for fault level calculations based on the Thevenin impedance estimation with those obtained from both the steady-state fault simulation (i.e., IEC 60909 standards) and dynamic simulations (i.e., RMS simulation) at different penetration of PE-based RESs. The outcome of this comparison would contribute to a better understanding of the impact of the increased penetration of RESs on the validity of using the fault level as a scanning tool reflecting the steady-state system strength represented by the Thevenin impedance. In other words, we intend to identify the extent to which the fault level results of the measure-based Thevenin impedance methods match with those obtained from the simulations. If they match, the results would indicate that the fault level at high penetration of RESs can still be employed as a reliable tool to scan the system strength, otherwise, the fault level-based approach may fail to do so. The adjusted IEEE nine-bus test system [33] was modelled in DIgSILENT PowerFactory. To consider multiple scenarios of penetration of RESs, a capacity-based metric for representing the percentage of the installed RESs in the system is defined, as given in Equation (8):

$$p\% = \frac{RESs}{SGs + RESs} \times 100\% \quad (8)$$

where $p\%$ is the penetration level percentage. SGs and RESs are the MVA ratings of the installed SGs and RESs, respectively.

Note that any RES penetration here is associated with SGs displacements (i.e., SGs decommissioning), hence the total installed generation capacity in the system is kept unchanged. The fault level is monitored at all load nodes (bus five, six, and eight), which represent three levels of system strength and Thevenin impedance seen from those nodes. Figure 4 shows the adjusted IEEE nine-bus test system which is modelled considering three different scenarios as follows:

(i) Scenario 1: base scenario with a total of 0% penetration of RESs.
(ii) Scenario 2: low penetration scenario with a total of 22% penetration of RESs (displacing SG-3 with PV system).
(iii) Scenario 3: high penetration scenario with a total of 56% penetration of RESs (displacing SGs-2 with type-four wind and SG-3 with PV system).

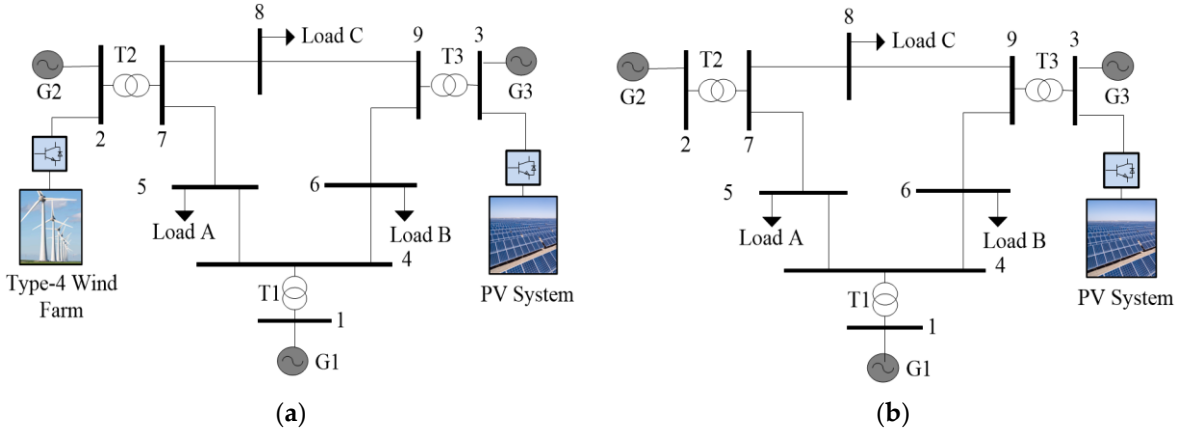

Figure 4. Modified IEEE nine-bus test system with RESs: (**a**) 22% RES penetration scenario (**b**) 56% RES penetration scenario.

Note that the total installed generation capacity equals to 567.5 MVA. The biggest generation unit at the G1, at slack bus one, is 247.5 MVA. The rest of the generation capacity

is divided into two values of 192 MVA and 128 MVA for G2 and G3, respectively. On the other hand, the system has three loads with a total of 315 MW and 115 MVAr located at a transmission network of 230 kV, as shown in Table 1.

Table 1. Load distribution in IEEE nine-bus test system.

Load	Bus	P [MW]	Q [MVAr]
Load A	Bus 5	125	50
Load B	Bus 6	90	30
Load C	Bus 8	100	35

5.1. Fault Level Results from the Load Change-Based Thevenin Impedance

This section calculates the fault level at the nodes of interest in the IEEE nine-bus test system using the estimated Thevenin impedance from using the load step change method described in Section 3.1. This has been achieved by scaling the loads at three different levels up to 105%, 110%, and 115% of their original values simultaneously. It is worth noting that both the active (P) and the reactive (Q) power of the loads have been changed correspondingly. Two sets of measurements for both the current and the voltage at each node of interest have been collected before and after the load change at a steady state, neglecting the transient. Three values of the Thevenin impedance are obtained using (5). The corresponding values of the fault level are calculated using (2), and are then averaged. Note that this has been repeated for each scenario of penetration of RESs as listed in Table 2.

It can be seen from Table 2 that the fault level results are marginally affected by the value of the load step change as they are almost converging to the same values for all buses, more specifically in scenarios one and two. However, the impact of the load step change might be more tangible in the third scenario where the penetration of RESs is the highest. This can be observed at bus eight, which is closer to the displaced SGs at G2 and G3. In other words, the sensitivity of the application of load change method for estimating the Thevenin impedance, and in turn the fault level, is location-dependent and it might be notably affected by the scenario of the penetration of RESs. As expected, a remarkable decrease in the fault level, and in turn the increased Thevenin impedance, can be observed by increasing the penetration level of RESs. For instance, the fault level at bus five has witnessed a decline from its original value of 934 MVA in scenario one (i.e., p = 0%), down to 717 MVA and 334 MVA in scenario two (i.e., p = 22%), and scenario three (i.e., p = 56%), respectively.

Table 2. Fault Level MVA obtained from the Load Change-based Thevenin Impedance.

	Scenario 1 (p = 0%)				Scenario 2 (p = 22%)				Scenario 3 (p = 56%)			
Bus Num.	105% Loading	110% Loading	115% Loading	Average	105% Loading	110% Loading	115% Loading	Average	105% Loading	110% Loading	115% Loading	Average
Bus 5	937	934	930	934	719	717	713	717	334	335	334	334
Bus 6	736	727	725	729	480	479	476	478	244	244	244	244
Bus 8	804	811	804	806	483	483	480	482	126	179	126	143

Similarly, the fault level at the other buses show a remarkable decline with more severity. For example, the fault level at bus six has decreased from 729 MVA in scenario one down to 478 MVA and 244 MVA in scenarios two and three, respectively. On the other hand, the highest decline in fault level was registered at bus eight, where the fault level decreased from 806 MVA in the base scenario (i.e., scenario one, p = 0%), down to 482 MVA and 143 MVA in scenarios two and three, correspondingly. This variable sensitivity of the fault level in different buses can be attributed to the fact that these nodes are located at different locations meaning that they have distinct electrical distances from the generation centers, which is also affected by the RES penetration scenario.

5.2. Fault Level Results from the Capacitor Switching-Based Thevenin Impedance

This part utilizes the capacitor switching events to collect required sets of measurements for estimating the Thevenin impedance of the system seen at three different buses (five, six, and eight). This is achieved by registering the steady-state voltages before and after switching on the capacitor bank at the studied nodes as detailed in Section 3.2. By using both the voltages with the reactive current injected by the capacitor bank, the Thevenin impedance can be calculated as previously described in (6). To do so, a 50 MVAr capacitor bank is switched on at each of the studied buses where the system strength represented by the Thevenin impedance is estimated. A voltage step change occurs, and the RMS positive sequence voltage is monitored without considering the impact of the transient and the inrush current. Table 3 lists the values of the calculated fault level at those buses by employing the estimated Thevenin impedances using (2). As shown in Table 3, it can be noted that the calculated values of the fault level are different from those calculated using the load change-based Thevenin impedance given in Table 2.

Table 3. Fault level MVA obtained from the capacitor bank switching-based Thevenin impedance.

Bus Num.	Scenario 1 (p = 0%)	Scenario 2 (p = 22%)	Scenario 3 (p = 56%)
Bus 5	979	924	794
Bus 6	914	794	742
Bus 8	958	779	395

This difference is not significant in scenario one (p = 0%) but it is getting larger with the increased penetration of RESs in scenarios two and three. For instance, the fault level at bus five witnessed a decline from its original value of 934 MVA in scenario one (i.e., p = 0%), down to 924 MVA and 794 MVA in scenario two (i.e., p = 22%), and scenario three (i.e., p = 56%), respectively. Similarly, the fault level at bus six has decreased from 914 MVA in scenario one down to 794 MVA and 742 MVA in scenarios two and three, respectively. Unlike the load change-based method, the calculated fault level at bus six does not show the same sensitivity to the high penetration of RESs, and those results in scenario two and scenario three are almost the same. On the other hand, the calculated fault level at bus eight has shown the highest sensitivity to the RES penetration scenario with the highest level of decline severity.

Taken together, these results show that the application of capacitor bank switching for estimating the Thevenin impedance, hence the fault level, is not only more sensitive to the location of the bus, but also to the RES penetration scenario. This might be attributed to the different sensitivity of the bus voltage to the local reactive current change other than the case of load change-based method, where both the active and reactive current are both changed for all loads simultaneously.

Generally, it can be noted that these two methods can estimate different values of Thevenin impedance and the fault level, hence, different system strength. To an extent, the difference might be marginal at the base scenario (i.e., scenario one, p = 0%), but this might be significant otherwise. For better evaluation and to provide a more accurate conclusion, the fault levels obtained from these methods are compared with the values obtained from the IEC 60909 standards and the dynamic simulations (i.e., RMS simulations), which is expected to be the most accurate one, in the next section.

5.3. Comparison Study Using the Adjusted IEEE Nine-Bus Test System

This section provides a comparison between the fault level results obtained from the previous methods that utilized measurement-based Thevenin impedance estimation for fault calculation, and those obtained from the steady-state and the dynamic simulations. To simplify the comparison process, the different fault level calculation approaches used in this study are abbreviated in Table 4.

Table 4. Abbreviations of fault level calculation methods.

Acronym	Method
LCTI	Load change-based Thevenin impedance
CSTI	Capacitor switching-based Thevenin impedance
IEC	Steady-state simulation based on IEC 60909
Simulation	Dynamic simulation based on RMS

As intended, this comparison aims to examine the extent to which the actual fault level can reflect the Thevenin impedance, hence the system strength in scenarios of high penetration of RESs. Figures 5–7, show the results obtained from measurement methods in comparison with the dynamic simulation in different penetration scenarios for bus five, six, and eight, respectively. Note that the steady-state simulation is based on IEC 60909 standards in which the fault current contribution of the PE-based RESs (i.e., PV and type-four wind) is accounted for as a current source. This contribution is added to the fault current of traditional SGs that is calculated based on the Thevenin equivalent method. The maximum values of the fault currents contribution to the PV system and the type-four wind generators are kept bounded by the maximum overrating capability of the converters (i.e., I_{Max}) around the rating current. In this study, a maximum fault current contribution of both installed RESs in the considered scenarios is set to 1.2 p.u. accordingly. It is worth mentioning that the actual fault current of the PE-based RESs during the faults may show different levels of contribution according to the severity of the fault and the measured voltage during the fault at the entry point connecting the RES to the grid. This also might be sensitive to the FRT and control strategy during the fault. In this research, for the dynamic simulation (RMS) purposes, the RESs are modelled and controlled in such a way to remain connected during the fault and to inject a reactive current proportional to the voltage dip seen by the RESs.

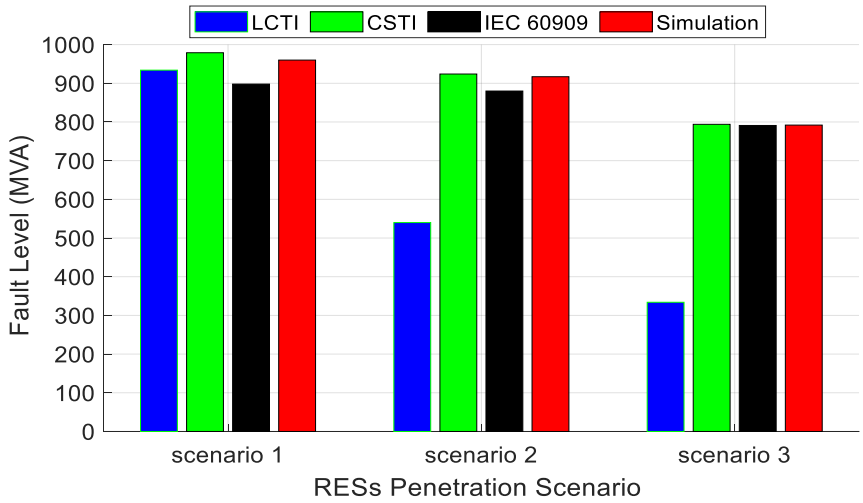

Figure 5. Bus five fault level in different penetration scenarios.

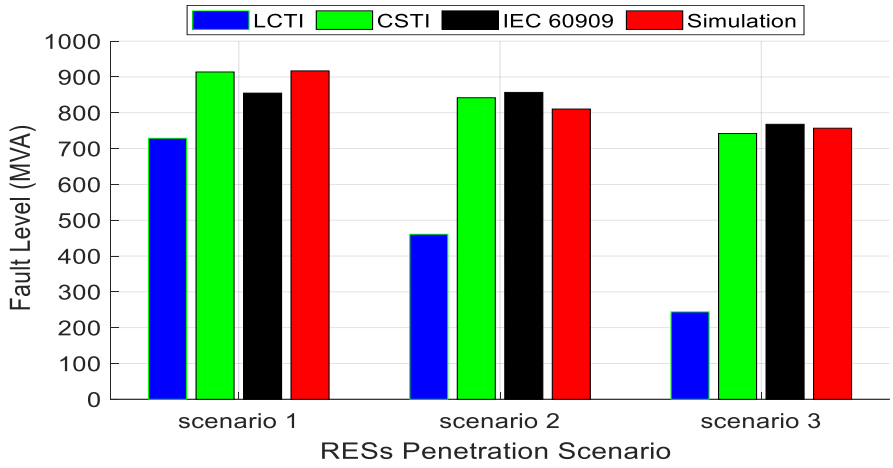

Figure 6. Bus six fault level in different penetration scenarios.

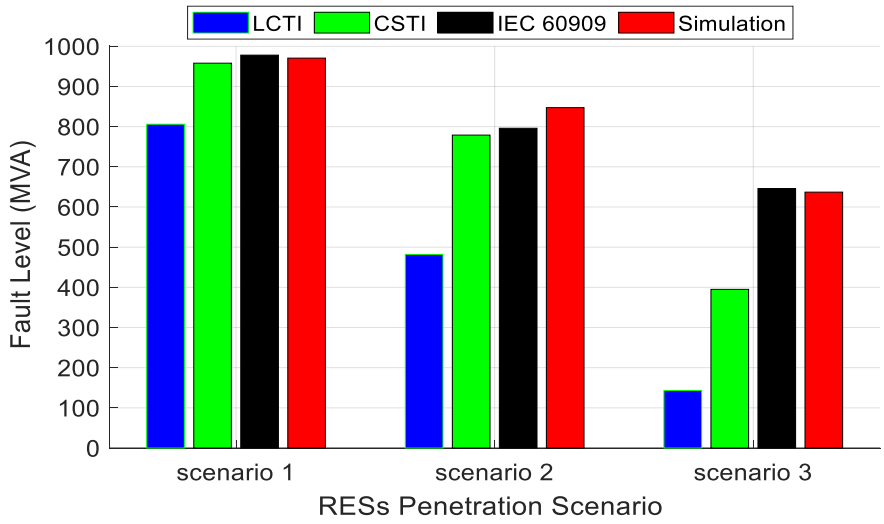

Figure 7. Bus eight fault level in different penetration scenarios.

Similar to the measurement-based fault calculation methods (i.e., LCTI and CSTI), both steady-state and dynamic simulations have shown the declining trends of the fault level with the increased penetration of RESs. While all the methods converge to the dynamic simulation results with a marginal difference in scenario one (i.e., no RES), a big mismatch can be observed in scenario two and scenario three. This can be seen more in bus eight, which is located between the G2 and G3 where the RESs are introduced.

Considering Figure 5, which presents the results obtained in bus five, both CSTI and IEC 60909 methods can lead to the same values of fault level which are matched with the dynamic simulations. However, the LCTI method has shown lower values of the fault level in scenarios one and two, hence a lower system strength. This means that the LCTI method does not account for the impact of the fault current contribution of the RESs. Likewise, the results obtained at bus six show that LCTI and IEC 60909 methods can converge with the dynamic simulation results opposing the LCTI method which underestimates the fault levels at high penetration of RESs (i.e., scenarios two and three) as shown in Figure 6. Based on that, it can be concluded that the LCTI may fail to represent the system strength at network buses.

As shown in Figure 7, the fault level obtained from LCTI at bus eight provided underestimated values compared with the dynamic simulations. Unlike the results of bus five and six, a different behavior can be observed at bus eight. For instance, although the fault level obtained by CSTI matched those obtained from dynamic simulation in scenarios one and two, it failed to do so in scenario three, with 56% penetration of RESs. Note that

both LCTI and CSTI methods fail to match the dynamic simulation results in scenario three with a larger gap for the results of LCTI.

The results of bus eight show that the measurement-based approaches assessed (LCTI and CSTI) reflect inaccurate system strength with high penetration of PE-based renewables. More specifically, they have shown lower system strength (i.e., higher Thevenin impedance) in comparison with what might be indicated from using the fault level results of the dynamic simulation. This also means that the CSTI method for fault level calculation is more sensitive to the location of the bus and the scenario of penetration of RESs. The closer the node to the RESs, the higher the mismatch between system strength indicated by the CSTI and the dynamic simulation. On the other hand, the steady-state simulation based on the IEC 60909 standards have shown the most accurate estimation of the dynamic simulation results regardless the scenario or the bus location. However, they might overestimate the actual fault level and the system strength at high penetration scenarios (scenarios two and three) depending on the location of the bus as shown in Figures 6 and 7.

In order to provide a better insight, the fault level results obtained from all utilized methods have been validated against the dynamic simulations. In this regard, the absolute error percentages corresponding to each method have been calculated for scenarios one, two, and three, and are listed in Tables 5–7, respectively. As depicted in Table 4, both CSTI and IEC 60909 methods have registered marginal errors with an average of 1.03% and 3.53%, respectively. On the other hand, the LCTI has a big error gap, with an average of 33.86%. Note that the maximum error associated with LCTI method is 57.8% at bus eight.

Table 5. Fault level MVA obtained in scenario one.

Bus Num.	Dynamic Simulation (MVA)	LCTI		CSTI		IEC 60909	
		MVA	Error%	MVA	Error%	MVA	Error%
Bus 5	960	934	2.7	979	2.0	898	6.5
Bus 6	917	540	41.1	924	0.8	880	4.0
Bus 8	792	334	57.8	794	0.3	791	0.1
Bus 6	917	482	47.4	779	15.0	796	13.2
Bus 8	792	143	81.9	395	50.1	646	18.4

Table 6. Fault level MVA obtained in scenario two.

Bus Num.	Dynamic Simulation (MVA)	LCTI		CSTI		IEC 60909	
		MVA	Error%	MVA	Error%	MVA	Error%
Bus 5	960	729	24.1	914	4.8	855	10.9
Bus 6	917	461	49.7	842	8.2	857	6.5
Bus 8	792	244	69.2	742	6.3	768	3.0

Table 7. Fault level MVA obtained in scenario three.

Bus Num.	Dynamic Simulation (MVA)	LCTI		CSTI		IEC 60909	
		MVA	Error%	MVA	Error%	MVA	Error%
Bus 5	960	806	16.0	958	0.2	978	1.9
Bus 6	917	482	47.4	779	15.0	796	13.2
Bus 8	792	143	81.9	395	50.1	646	18.4

Table 5 shows that the error between the IEC 60909 method and the dynamic simulation is increasing, and that the maximum error at bus eight has increased from (6.5%, in scenario one) to (10.9%, in scenario two). Table 6 has revealed that all methods have increased error in scenario three when compared with the dynamic simulations. For example, very large errors have been registered at all the studied buses when using LCTI and CSTI

methods with an average of 48.33% and 21.76%, respectively. Nevertheless, the results of the IEC 609 standards method have still the closest results to the dynamic simulations with less error, and the average error is limited to 11.16%.

6. Conclusions

In this paper, the relationship between the fault level and the system strength in future grid scenarios of high penetration of PE-based RESs is examined. Our assessment has included comparison of the measurement-based methods proposed by the up-to-date literature for estimation of the Thevenin impedance at different nodes with the IEC 60909 methods and dynamic simulations using the adjusted IEEE nine-bus test system modelled in DIgSILENT PowerFactory. The measurement-based methods have been utilized for calculating the fault level, hence scanning the system strength. This has been achieved by creating a perturbation caused by load change and capacitor switching for generating measurement sets that are required for estimating the Thevenin impedance at different nodes in the system. The fault level was calculated using steady-state simulations based on IEC 60909 standards which employ the Thevenin equivalent and account for the fault current contributions from PE-based RESs. The fault level calculated using load change-based Thevenin impedance (LCTI), capacitor switching-based Thevenin impedance (CSTI), and IEC 60909 methods have been compared with the actual fault level results obtained from the dynamic simulations considering three different scenarios of RES penetrations (p = 0%, p = 22% and p = 56%). This comparison has aimed to investigate the extent to which these methods can represent the Thevenin impedance correctly, hence a valid system strength estimation in future scenarios with high penetration of RESs.

The results have shown that the system strength, either indicated by the steady-state Thevenin impedance or the fault level in faulty conditions, has been affected significantly by the increased penetration of RESs and the displacement of SGs. It has also been shown that the concept of fault level and system strength can still be interchangeably used to represent each other in scenarios of low penetration of RESs. However, this might not be valid when increasing the penetration of RESs and displacing large central SGs. In other words, although the PE-based RESs might contribute to the system strength at steady-state conditions, their different behaviour during faulty conditions might not reflect this contribution properly. Hence, the fault level in scenarios of high penetration of RESs might not be an accurate measure of the system strength and vice versa.

Furthermore, the results obtained have shown that the fault level calculated based on the measurement-based methods (i.e., LCTI and CSTI) cannot lead to the same conclusion about the system strength. Regardless of the difference between the results of LCTI and CSTI methods in representing the system strength, they have shown very low values of fault level, hence system strength, when compared with dynamic simulations at high penetration scenarios of RESs. It can be concluded that the steady-state system strength, if indicated by the actual fault level obtained from the dynamic simulations, is overestimated, which necessitates the need to differentiate between these two concepts in future scenarios.

In terms of the fault level calculated using the steady-state simulations based on the IEC 60909 standards, it can be concluded that the accuracy of the results might not be satisfactory when considering scenarios of high penetration of RESs, but still can provide a much better insight about the fault level in faulty conditions.

Author Contributions: Conceptualization, R.A. and Q.S.; Methodology, R.A., H.M., M.A.-O. and S.H.; Software, R.A., S.A. and S.H.; Validation, R.A., M.K. and H.M.; Formal analysis, R.A. and S.H.; Investigation, R.A., M.K., H.M., S.A., M.A.-O. and Q.S.; Resources, M.K.; Data curation, R.A. and M.A.-O.; Writing—original draft, R.A. and H.M.; Writing—review & editing, M.K., H.M., S.A., Q.S. and S.H.; Visualization, R.A. and M.K.; Supervision, M.K.; Project administration, M.K.; Funding acquisition, M.K. All authors have read and agreed to the published version of the manuscript.

Funding: This research received no external funding.

Informed Consent Statement: Not applicable.

Data Availability Statement: We will share it in Google Scholar and ResearchGate.

Conflicts of Interest: The authors declare no conflict of interest.

References

1. Vinaya Mohanan, V.A.; Mareels, I.M.; Evans, R.J.; Morton, A.B.; Kolluri, R.R. Stability and bifurcations in low inertia PV rich power networks. *IET Gener. Transm. Distrib.* **2020**, *14*, 6122–6132. [CrossRef]
2. Aljarrah, R.; Marzooghi, H.; Yu, J.; Terzija, V. Monitoring of fault level in future grid scenarios with high penetration of power electronics-based renewable generation. *IET Gener. Transm. Distrib.* **2021**, *15*, 294–305. [CrossRef]
3. Milano, F.; Dörfler, F.; Hug, G.; Hill, D.J.; Verbič, G. Foundations and challenges of low-inertia systems. In Proceedings of the 2018 Power Systems Computation Conference (PSCC), Dublin, Ireland, 11–15 June 2018.
4. Aljarrah, R.R. Assessment of Fault Level in Power Systems with High Penetration of Non-Synchronous Generation. Ph.D. Thesis, The University of Manchester, Manchester, UK, 2020.
5. Hodge, B.M.S.; Jain, H.; Brancucci, C.; Seo, G.S.; Korpås, M.; Kiviluoma, J.; Holttinen, H.; Smith, J.C.; Orths, A.; Estanqueiro, A.; et al. Addressing technical challenges in 100% variable inverter-based renewable energy power systems. *Wiley Interdiscip. Rev. Energy Environ.* **2020**, *9*, 376. [CrossRef]
6. Gu, H.; Yan, R.; Saha, T. Review of system strength and inertia requirements for the national electricity market of Australia. *CSEE J. Power Energy Syst.* **2019**, *5*, 295–305.
7. Urdal, H.; Ierna, R.; Zhu, J.; Ivanov, C.; Dahresobh, A.; Rostom, D. System strength considerations in a converter dominated power system. *IET Renew. Power Gener.* **2015**, *9*, 10–17. [CrossRef]
8. Kanálik, M.; Margitová, A.; Beňa, Ľ.; Kanáliková, A. Power system impedance estimation using a fast voltage and current changes measurements. *Energies* **2020**, *14*, 63. [CrossRef]
9. Aljarrah, R.; Marzooghi, H.; Yu, J.; Terzija, V. Sensitivity analysis of transient short circuit current response to the penetration level of non-synchronous generation. *Int. J. Electr. Power Energy Syst.* **2021**, *125*, 106556. [CrossRef]
10. Short-Circuit Currents in Three-Phase Ac Systems, Part 0: Calculation of Currents. 2016. Available online: https://webstore.iec.ch/publication/24100 (accessed on 20 November 2022).
11. Recommended Practice for Calculating Ac Short-Circuit Currents in Industrial and Commercial Power Systems. 2006. Available online: https://ieeexplore.ieee.org/document/4015546 (accessed on 20 November 2022).
12. Fonseca, A.; Salazar, G.; Quilumba, F.; Pérez-Yauli, F. Determination of the Thevenin equivalent in power grids using real records based on short circuit power. *IET Gener. Transm. Distrib.* **2021**, *15*, 13–23. [CrossRef]
13. De Meerendre, M.K.; Prieto-Araujo, E.; Ahmed, K.H.; Gomis-Bellmunt, O.; Xu, L.; Egea-Àlvarez, A. Review of local network impedance estimation techniques. *IEEE Access* **2020**, *8*, 213647–213661. [CrossRef]
14. Mohammed, N.; Kerekes, T.; Ciobotaru, M. An online event-based grid impedance estimation technique using grid-connected inverters. *IEEE Trans. Power Electron.* **2020**, *36*, 6106–6117. [CrossRef]
15. Yuan, H.; Li, F. A comparative study of measurement-based Thevenin equivalents identification methods. In Proceedings of the 2014 North American Power Symposium (NAPS), Pullman, WA, USA, 7–9 September 2014.
16. Kanálik, M.; Kolcun, M. September. The principle of actual short-circuit power determination in different nodes of the power system. In Proceedings of the 7th International Scientific Symposium on Electrical Power Engineering (Elektroenergetika 2013), Stará Lesná, Slovakia, 18–20 September 2013.
17. Zhang, Y.; Huang, S.H.F.; Schmall, J.; Conto, J.; Billo, J.; Rehman, E. Evaluating system strength for large-scale wind plant integration. In Proceedings of the 2014 IEEE PES General Meeting, National Harbor, MD, USA, 27–31 July 2014.
18. Kim, D.; Cho, H.; Park, B.; Lee, B. Evaluating influence of inverter-based resources on system strength considering inverter interaction level. *Sustainability* **2020**, *12*, 3469. [CrossRef]
19. Huang, L.; Xin, H.; Li, Z.; Ju, P.; Yuan, H.; Wang, G. Identification of generalized short-circuit ratio for on-line stability monitoring of wind farms. *IEEE Trans. Power Syst.* **2020**, *35*, 3282–3285. [CrossRef]
20. Zhang, F.; Xin, H.; Wu, D.; Wang, Z.; Gan, D. Assessing strength of multi-infeed LCC-HVDC systems using generalized short-circuit ratio. *IEEE Trans. Power Syst.* **2018**, *34*, 467–480. [CrossRef]
21. Gavrilovic, A. AC/DC system strength as indicated by short circuit ratios. In Proceedings of the International Conference on AC and DC Power Transmission, London, UK, 17–20 September 1991.
22. Yu, L.; Sun, H.; Xu, S.; Zhao, B.; Zhang, J. Critical system strength evaluation of the power system with high penetration of renewable energy generations. *CSEE J. Power Energy Syst.* **2021**, *8*, 710–720.
23. Gomis-Bellmunt, O.; Song, J.; Cheah-Mane, M.; Prieto-Araujo, E. Steady-state impedance mapping in grids with power electronics: What is grid strength in modern power systems? *Int. J. Electr. Power Energy Syst.* **2022**, *136*, 107635. [CrossRef]
24. Gordon, S.; Bell, K.; Hong, Q. Implications of reduced fault level and its relationship to system strength: A Scotland case study. In *CIGRE Session*; International Council on Large Electric Systems: Paris, France, 2022.
25. Abdelkader, S.M.; Morrow, D.J. Online Thévenin equivalent determination considering system side changes and measurement errors. *IEEE Trans. Power Syst.* **2014**, *30*, 2716–2725. [CrossRef]
26. Pourbagher, R.; Derakhshandeh, S.Y.; Golshan, M.E.H. A novel method for online voltage stability assessment based on PMU measurements and Thevenin equivalent. *IET Gener. Transm. Distrib.* **2022**, *16*, 1780–1794. [CrossRef]

27. Abdelkader, S.M.; Morrow, D.J. Online tracking of Thévenin equivalent parameters using PMU measurements. *IEEE Trans. Power Syst.* **2012**, *27*, 975–983. [CrossRef]
28. Lee, Y.; Han, S. Real-time voltage stability assessment method for the Korean power system based on estimation of Thévenin equivalent impedance. *Appl. Sci.* **2019**, *9*, 1671. [CrossRef]
29. Bahadornejad, M.; Ledwich, G. System Thevenin impedance estimation using signal processing on load bus data. In Proceedings of the 6th International Conference on Advances in Power System Control, Operation and Management, Hong Kong, China, 11–14 November 2003.
30. Arefifar, S.A.; Xu, W. Online tracking of power system impedance parameters and field experiences. *IEEE Trans. Power Deliv.* **2009**, *24*, 1781–1788. [CrossRef]
31. Sun, T.; Li, Z.; Rong, S.; Lu, J.; Li, W. Effect of load change on the Thevenin equivalent impedance of power system. *Energies* **2017**, *10*, 330. [CrossRef]
32. Patcharoen, T.; Ngaopitakkul, A. Transient inrush current detection and classification in 230 kV shunt capacitor bank switching under various transient-mitigation methods based on discrete wavelet transform. *IET Gener. Transm. Distrib.* **2018**, *12*, 3718–3725. [CrossRef]
33. Vittal, V.; McCalley, J.D.; Anderson, P.M.; Fouad, A.A. *Power System Control and Stability*; John Wiley & Sons: Hoboken, NJ, USA, 2019.